Printed in the Republic of Korea
ANALYTICAL SCIENCE & TECHNOLOGY
Vol. 39 No. 4, 266-277, 2026
https://doi.org/10.5806/AST.2026.39.4.266

Separation of elagolix atropisomers by supercritical fluid chromatography combined with calculation of rotational energy barriers

Jun Wang[1], Hongliang Wen[1], Chuanlong Zeng[2], Rongwen Weng[1], Jian Le[1], Dongying Chen[2,★], and Hao Liu[1,★]

[1]*Shanghai Institute for Drug Control, Shanghai 201203, China*
[2]*Shanghai Institute of Materia Medica, Chinese Academy of Sciences, Shanghai, 201203, China*
(Received June 18, 2026; Revised July 27, 2026; Accepted August 3, 2026)

Abstract: Elagolix, a GnRH antagonist for endometriosis-associated pain, exhibits two atropisomers due to hindered rotation about its C5–C16 bond. Separating these atropisomers is crucial for drug development and quality control. Although rotational energy barriers are the key parameters governing the interconversion kinetics of atropisomers, studies that correlate these calculated values to chromatographic behavior are relatively limited. This study integrates green supercritical fluid chromatography (SFC) with quantum chemical calculations to explore this relationship. An SFC method was optimized, achieving good separation of the two atropisomers of elagolix (Rs > 2.0) within 15 min. Quantum chemical calculations revealed rotational energy barriers of 23~26 kcal/mol, with half-lives ranging from minutes to days, placing elagolix into Class II of the LaPlante classification. Experimentally, the changes in the interconversion plateau under different temperature conditions showed good consistency with the calculated kinetic trends. By integrating chromatographic experiments with rotational energy barrier calculations, this study provides mechanistic insights into the separation behavior of elagolix atropisomers and may provide information for understanding the potential separability of other atropisomeric drugs.

Keywords: elagolix, atropisomers, supercritical fluid chromatography (SFC), quantum chemical, rotational energy barriers

1. Introduction

Elagolix (Orilissa™), approved by the FDA in 2018, is the first oral non-peptide gonadotropin-releasing hormone (GnRH) receptor antagonist for endometriosis-associated pain.[1-3] Its molecular formula is $C_{32}H_{29}F_5N_3O_5Na$, with a molecular weight of 653.58 g/mol for the sodium salt and 631.60 g/mol for the free acid. Atropisomers arise from restricted rotation about the C5–C16 bond, due to steric and electronic repulsion involving the ortho-fluorophenyl, 6-methyl, and 4-carbonyl groups (*Fig.* 1).[4] Without a reliable analytical method for monitoring atropisomers, batch-to-batch variation in atropisomer composition

★ Corresponding author
Phone : +82-(0)86-21-5080-6600 Fax : +82-(0)
E-mail : dychen@mail.shcnc.ac.cn (D. Chen), liuhao1968@hotmail.com (H. Liu)

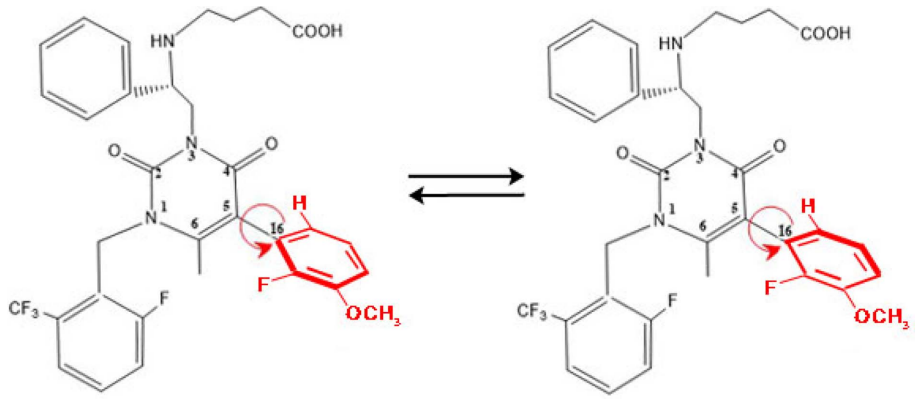

Fig. 1. Illustration of the two atropisomers of elagolix (free acid form). The atropisomers arise from restricted rotation about the single bond indicated by the red arrow.

may compromise process reproducibility and scale-up robustness. Moreover, the two atropisomers may exhibit different pharmacological activities, potentially skewing efficacy and safety assessments and complicating drug development.[5-8] Therefore, establishing an analytical method for resolving and monitoring elagolix atropisomers is important.

Atropisomer is a form of axial chirality arising from restricted rotation about a bond, and interconversion between atropisomers requires the overcoming of a rotational energy barrier.[9,10] Owing to their conformational differences, individual atropisomers may exhibit distinct pharmacokinetic, pharmacodynamic, or toxicological profiles, thereby directly influencing the overall efficacy and safety of a drug.[11] Moreover, atropisomers may interconvert under physiological conditions. Although quality-control requirements for centrally chiral drugs are well established, axially chiral drugs that exist as atropisomers have received comparatively less attention.[12-14] Reports on their resolution remain scarce, and analytical methods for their separation are still underdeveloped. Consequently, efficient separation, reliable identification and quantification of atropisomers are urgently required in chiral pharmaceutical analysis, essential not only for drug development and quality assurance but also for toxicological evaluation and regulatory compliance.[15-22]

Atropisomer separations currently rely primarily on three analytical techniques: high-performance liquid chromatography (HPLC), supercritical fluid chromatography (SFC), and capillary electrophoresis (CE). HPLC, particularly in normal-phase mode, typically requires large volumes of expensive and toxic solvents such as n-hexane.[23] CE uses aqueous-based mobile phases and may face solubility limitations for hydrophobic drugs such as elagolix.[24,25] In contrast, SFC typically uses supercritical CO_2 and a small proportion of an alcohol (e.g., methanol or ethanol), thereby reducing organic-solvent consumption and environmental burden.[26,27] Therefore, SFC was chosen to separate elagolix atropisomers. To better understand the relationship between atropisomer interconversion and chromatographic behavior, this study combined SFC experiments with quantum chemical calculations.

In this study, an environmentally friendly SFC method was developed for the separation of elagolix atropisomers. Quantum chemical calculations were used to estimate the rotational energy barriers in methanol and ethanol at temperatures ranging from 303 to 313 K and to explore their relationship with the observed chromatographic separation behavior. This integrated experimental and computational approach provides insight into the separation and interconversion behavior of elagolix atropisomers and may support method development for other atropisomeric drugs.

2. Experimental

2.1. Materials and instrumentation

Elagolix (purity 99.08 %) was purchased from TargetMol Chemicals Inc (Shanghai, China). HPLC-grade methanol, ethanol, acetonitrile, and isopropanol were purchased from Sigma-Aldrich (Shanghai, China). Carbon dioxide (CO_2, purity 99.99 %) was obtained from Air Liquide (Shanghai, China).

All supercritical fluid chromatography (SFC) analyses were performed on a Waters ACQUITY Ultra Performance Convergence Chromatography (UPC^2) system equipped with a photodiode array (PDA) detector.

The following chiral columns were evaluated: Waters ACQUITY UPC^2 Trefoil CEL1, CEL2, and AMY1 (3.0 mm × 150 mm, 2.5 μm); Daicel CHIRALPAK AD-H and OD-H (4.6 mm × 250 mm, 5 μm); Welch Ultimate AMY-S, AMY-D, and Cellu-J (4.6 mm × 250 mm, 5 μm).

The final optimized SFC conditions were as follows:

Mobile phase: CO_2–ethanol (70:30, v/v); Column temperature: 35 °C; Backpressure: 13.8 MPa; Flow rate: 1.0 mL/min; Injection volume: 5 μL; Detection wavelength: 274 nm.

2.2. Solution preparation and analytical method validation

2.2.1. Stock solution

Approximately 10 mg of elagolix was accurately weighed and transferred into a 50 mL volumetric flask. Methanol was added, and the mixture was sonicated until complete dissolution. The volume was then made up to the mark with methanol and mixed thoroughly to obtain a stock solution at a concentration of 0.2 mg/mL.

2.2.2. Analytical method validation

Because individual reference standards for the two elagolix atropisomers were not available, quantitative validation was performed for total elagolix. The total integrated response was defined as the sum of the integrated areas of Peak 1, the interconversion plateau, and Peak 2:

$$A_{total} = A_{peak1} + A_{plateau} + A_{peak2}$$

The Peak 1/Peak 2 area ratio (P_1/P_2 ratio) and chromatographic resolution (R_S) were additionally monitored as indicators of separation reproducibility.

Linearity was evaluated at five concentration levels covering 10–200 μg/mL (10, 20, 50, 100, 200 μg/mL). Each solution was injected in triplicate. The calibration curve was constructed by least-squares linear regression of the total integrated response against the nominal total elagolix concentration.

The LOD and LOQ were estimated at signal-to-noise (S/N) ratios of approximately 3 and 10, respectively. The lower-intensity peak was used as a conservative criterion to ensure the detectability of both atropisomer peaks.

Repeatability was evaluated using six independently prepared sample solutions at the nominal test concentration of 50 μg/mL. The solutions were analyzed by the same analyst under the same operating conditions on the same day. Intermediate precision was evaluated using a second set of six independently prepared solutions analyzed on a different day by a second analyst. The total integrated response, P_1/P_2 ratio and R_S were evaluated. The results from all 12 preparations were pooled to calculate the overall intermediate-precision RSD.

Accuracy was evaluated at 40, 50, and 60 μg/mL, corresponding to 80 %, 100 %, and 120 % of the nominal test concentration, respectively. Three independently prepared samples were analyzed at each level. The total elagolix concentration was back-calculated from the calibration curve, and recovery was calculated. Mean recovery and RSD were calculated at each concentration level.

Robustness was evaluated by introducing small deliberate variations in the chromatographic conditions, including flow rates of 0.9 and 1.1 mL/min, organic-modifier contents of 29 % and 31 % (v/v), and back-pressure settings of 13.6 and 13.9 MPa. Each parameter was varied individually while the remaining conditions were maintained at their nominal settings. The total integrated response and P_1/P_2 ratio were monitored.

Solution stability was evaluated by storing the sample solutions at 25 °C and analyzing them at 0, 24 and 48 h. At each time point, the total integrated response and P_1/P_2 ratio were monitored.

Chromatographic data were processed using Empower software. The same processing method and integration parameters were applied to all chromatograms. Peak 1, the interconversion plateau, and Peak 2 were integrated separately using predefined and consistent integration boundaries.

2.3. Conformational search and stationary point optimization

Elagolix is formulated as a sodium salt to improve solubility and formulation performance. The free acid form was selected for quantum chemical calculations because it provides a well-defined molecular structure for conformational analysis and is relevant to the molecular species involved in atropisomerism under physiological conditions. In addition, elagolix sodium may dissociate or convert to the corresponding acid form upon exposure to physiological media. Therefore, rotational energy barriers ($\Delta G^{\ddagger}$) and interconversion kinetics were estimated using the free acid form.

Conformational search and geometry optimization: Conformational sampling of elagolix in methanol and ethanol was performed using the MacroModel module (Schrödinger Suite) with its torsional search algorithm.[28] The lowest-energy conformer was further optimized at the B3LYP-D3(BJ)/6-31G(d,p) level in Gaussian 16 employing the SMD (Solvation model based on density) solvation model.[29]

Relaxed potential energy surface (PES) scan: To locate stationary points along the rotational coordinate of the phenyl-containing dihedral, a relaxed potential energy surface scan (360°, 10° increments) was conducted using the semi-empirical GFN2-xTB method via the gau_xtb interface. [30,31] The resulting minima and maxima served as initial geometries for subsequent DFT optimization at the same B3LYP-D3(BJ)/6-31G(d,p) level.

Transition state (TS) location and verification: All optimized structures were verified by vibrational frequency analysis. Minima showed no imaginary frequencies, and each transition state exhibited exactly one imaginary frequency corresponding to the targeted phenyl rotation. When spurious methyl rotations interfered, a constrained dihedral optimization was applied to correct the reaction vector before final refinement. This procedure ensured that all transition states correctly connect the corresponding reactant and product minima.

2.4. Rotational energy barrier calculation

High-precision single-point energies were computed at the ωB97X-D/def2-TZVP level using B3LYP-D3(BJ)/6-31G(d,p)-optimized geometries. Thermal corrections at 303, 308 and 313 K were derived from frequency analyses at the same level via Shermo program and combined with the ωB97X-D single-point energies to obtain final Gibbs free energies.[32-34] Frequency scaling factors were applied to minimize harmonic approximation errors.

2.5. Determination of the rate constant (k_1) and half-life ($t_{1/2}$)

The transition state theory form of the Eyring equation was applied to analyze the reaction kinetics:

$$\Delta G^{\ddagger} = -RT\ln\left(\frac{k_1 h}{\kappa k_R T}\right)$$

Where $\Delta G^{\ddagger}$ is the Gibbs free energy of activation (J/mol); R is the ideal gas constant (8.3145 J/mol/K); T is the absolute temperature (K); k_1 is the rate constant (s^{-1}); κ is the transmission coefficient (taken as 1.0 in this work); k_B is the Boltzmann constant (1.381×10^{-23} J/K); h is Planck's constant (6.626×10^{-34} J·s).

To determine k_1 from a given $\Delta G^{\ddagger}$,[35-38] the equation was rearranged as follows:

1. Rearrangement of the equation:

$$\ln\left(\frac{k_1 h}{\kappa k_R T}\right) = -\frac{\Delta G^{\ddagger}}{RT}$$

2. Solving for k_1:

$$k_1 = \frac{\kappa k_B T}{h} \exp\left(\frac{\Delta G^{\ddagger}}{RT}\right)$$

3. The half-life ($t_{1/2}$) was then calculated using:

$$t_{1/2} = \frac{ln2}{k_1}$$

3. Results and Discussion

3.1. Method development and optimization

3.1.1. Screening of chiral stationary phases

Unlike configurationally stable enantiomers, atropisomers may undergo dynamic interconversion under chromatographic conditions. Effective separation therefore requires sufficient stereochemical discrimination while minimizing interconversion during analysis. Accordingly, we systematically evaluated chiral stationary phases (CSPs) and key chromatographic variables, including mobile-phase composition and column temperature.

The Trefoil CEL2 column, which contains 3-chloro-4-methylphenyl carbamate substituents, provided the best separation performance for elagolix atropisomers (*Fig.* 2A), in contrast, stationary phases bearing symmetrical 3,5-dimethyl substituents showed insufficient resolution, possibly because their relatively homogeneous and less polar chiral environments may provide weaker differential interactions with the two atropisomeric conformations (*Fig.* 2B-E). The benzoate-type stationary phase (*Fig.* 2F), whose recognition is generally dominated by π–π interactions, produced a single severely tailing peak, suggesting that its interaction mode may not be well matched with the structural features of elagolix atropisomers. The mixed-type phases (*Fig.* 2G, H) yielded sharp but poorly resolved peaks, which may reflect limited atropisomeric selectivity under the tested conditions (*Table* 1).

The higher atropisomer resolution obtained on Trefoil CEL2 may be associated with the 3-chloro-4-methylphenylcarbamate substituent of its cellulose-based chiral stationary phase (*Fig.* 3). This substitution pattern may modify both the local steric profile and the electrostatic potential of the phenylcarbamate recognition environment. The two atropisomers of elagolix present their polar functional groups and aromatic surfaces in different three-dimensional

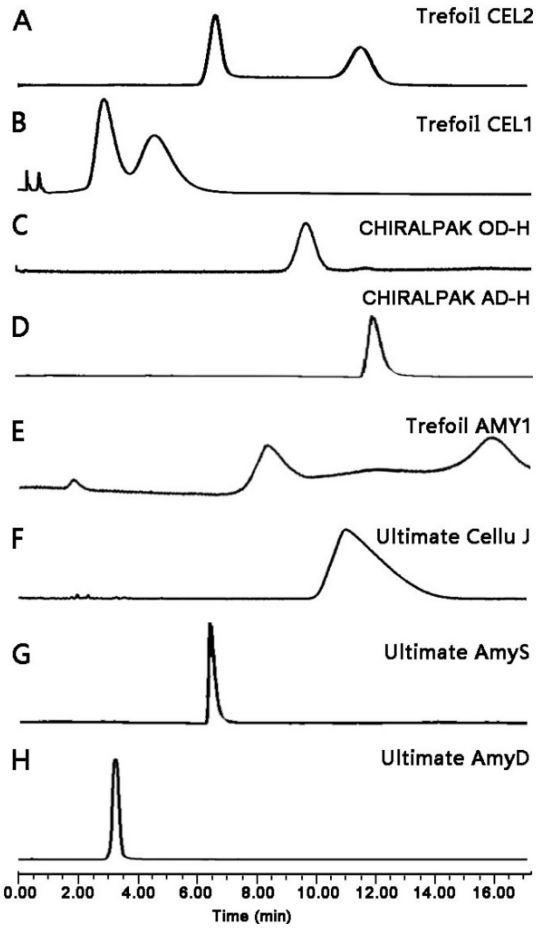

Fig. 2. Screening of chiral stationary phases for the separation of elagolix atropisomers. *Only the CEL2 phase achieved baseline resolution (*Rs* > 2.0).

Table 1. Summary of chiral stationary phase recognition toward elagolix atropisomers.

Stationary Phase	Backbone	Derivatization	Cavity Feature	Performance
Trefoil CEL2	Cellulose	Carbamate (**3-Cl, 4-CH_3**)	Electrostatic/steric gradient	✓**Good separation**
CEL1/OD-H/AD-H/ AMY1	Cellulose/ Amylose	Carbamate (3, 5-di-CH_3)	Homogeneous, low polarity	✗Poor separation
Cellu J	Cellulose	Benzoate (-CH_3)	π-π stacking	✗Single tailing peak
AmyS/AmyD	Amylose	Mixed benzoate/ phenyl carbamate	Diffuse, averaged	✗Single sharp peak

orientations and may therefore establish different combinations of hydrogen-bonding, dipole-related, dispersion, and steric interactions with the CEL2 stationary phase, resulting in differential stereochemical matching and retention. A directional C–Cl···O contact may also contribute as a secondary interaction. However, the chromatographic data alone do not confirm the proposed mechanism. Further computational, spectroscopic, or thermodynamic studies would be required to clarify the detailed recognition mechanism.

Using the Trefoil CEL2 column, two resolved peaks were obtained with a distinct plateau region between them (*Fig.* 2A). This result suggests the occurrence of on-column interconversion between the two atropisomers. This interpretation is supported by previous studies in which similar plateau behavior was observed in dynamic chromatographic systems involving interconvertible stereoisomers.[39-42]

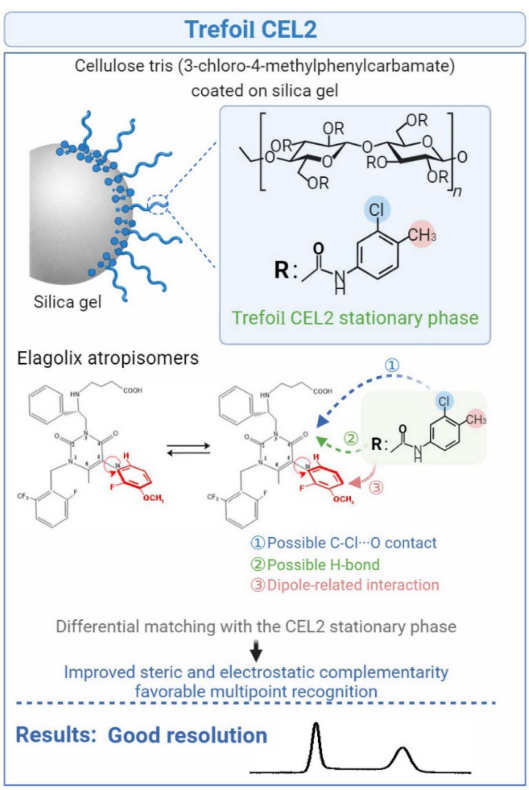

Fig. 3. Proposed qualitative multipoint-recognition model for the separation of elagolix atropisomers on the Trefoil CEL2 stationary phase.

3.1.2. Optimization of chromatographic conditions

After selecting Trefoil CEL2 as the optimal chiral stationary phase, key SFC parameters, including the organic modifier, modifier proportion, column temperature, flow rate and backpressure were optimized to balance resolution, analysis time, and method greenness.

Different organic modifiers were evaluated to improve elution strength and stereoselectivity. Acetonitrile led to delayed elution with weak response (*Fig.* 4C), whereas isopropanol failed to elute the analytes under the tested conditions (*Fig.* 4D). In contrast, both methanol and ethanol enabled effective resolution of the two atropisomers (*Fig.* 4A, B). Ethanol was selected as the preferred modifier because it provided comparable separation performance while offering lower toxicity, renewable sourcing, and reduced environmental impact, which are consistent with the principles of green analytical chemistry.

The ethanol proportion was then optimized to balance resolution and analysis time (*Fig.* 4E–H). A low ethanol content resulted in broad peaks and prolonged retention, whereas excessive ethanol (40 %) led to rapid elution with reduced resolution. The use of 30 % ethanol provided the best balance between resolution, peak shape, and analysis time, and was therefore selected for subsequent experiments.

Column temperature was also considered during method optimization because it affects the interconversion behavior of atropisomers. A working temperature of 35 °C was selected as a suitable compromise. At this temperature, the plateau contribution remained limited, while sufficient resolution and acceptable peak shape were maintained (*Fig.* 5). In addition, this moderate temperature is close to routine laboratory operating conditions and may help reduce energy consumption compared with higher-temperature operation.

The flow rate and backpressure were further considered to ensure stable SFC operation and reproducible retention. A flow rate of 1.0 mL/min and a backpressure of 13.8 MPa were adopted

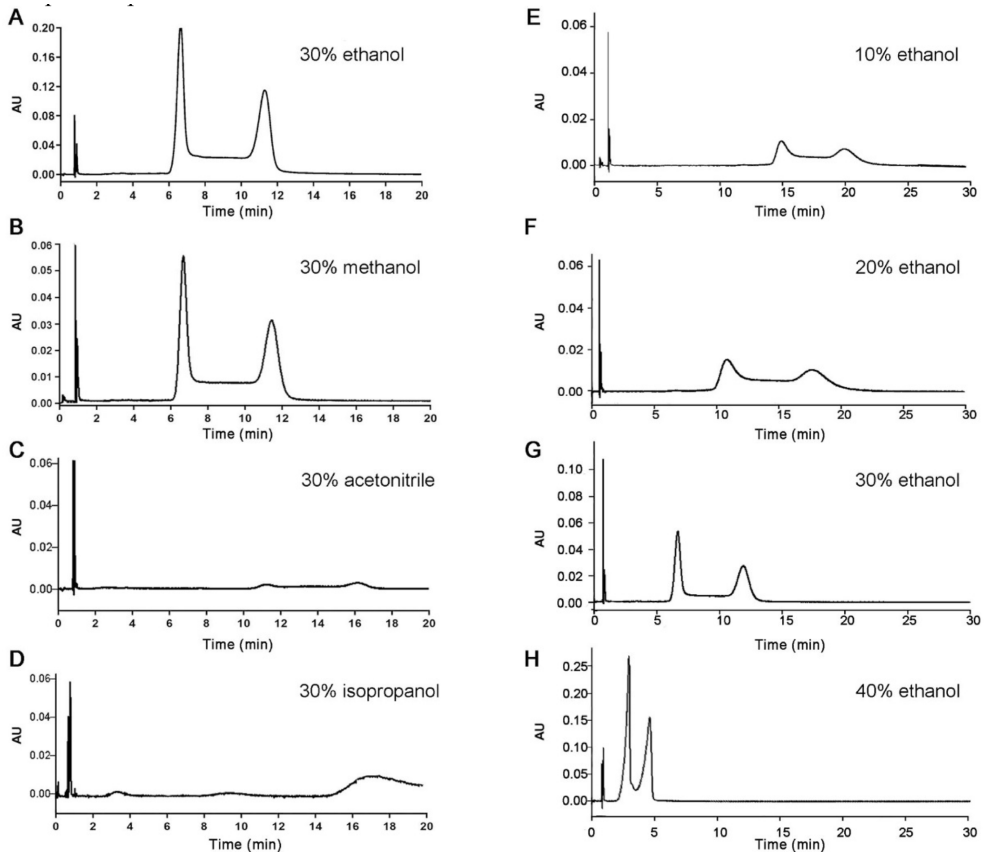

Fig. 4. Screening of organic modifier type and proportion. (A–D) Ethanol, methanol, acetonitrile, and isopropanol, each at 30 % (v/v), respectively. (E–H) Ethanol at 10 %, 20 %, 30 %, and 40 % (v/v), respectively.

because further adjustment of these parameters did not improve separation performance under the tested conditions.

The detection wavelength was selected based on the UV absorption profile of elagolix. Although stronger absorbance was observed at 208 nm, 274 nm was chosen to reduce potential interference and baseline noise from organic modifiers in the low-UV region and to improve method specificity.

Based on the systematic optimization described above, the final optimized SFC conditions were as follows: separation was performed on a Trefoil CEL2 column (3.0 mm × 150 mm, 2.5 μm) using a mobile phase of CO_2–ethanol (70:30, v/v) at a flow rate of 1.0 mL/min and a backpressure of 13.8 MPa. The column temperature was maintained at 35 °C, detection was set at 274 nm, and the injection volume was 5 μL.

Interestingly, a distinct plateau region was observed between the two resolved peaks, indicating partial on-column interconversion (*Fig.* 5). As the column temperature increased from 30 to 45 °C, the plateau area progressively increased from approximately 8 % to 40 % (*Fig.* 5I-J). This trend suggests that elevated temperature accelerates atropisomer interconversion during chromatographic migration. The temperature dependent changes in the plateau area therefore provide important experimental evidence for the dynamic interconversion behavior of elagolix atropisomers and serve as the basis for comparison with the quantum chemical calculations described below.

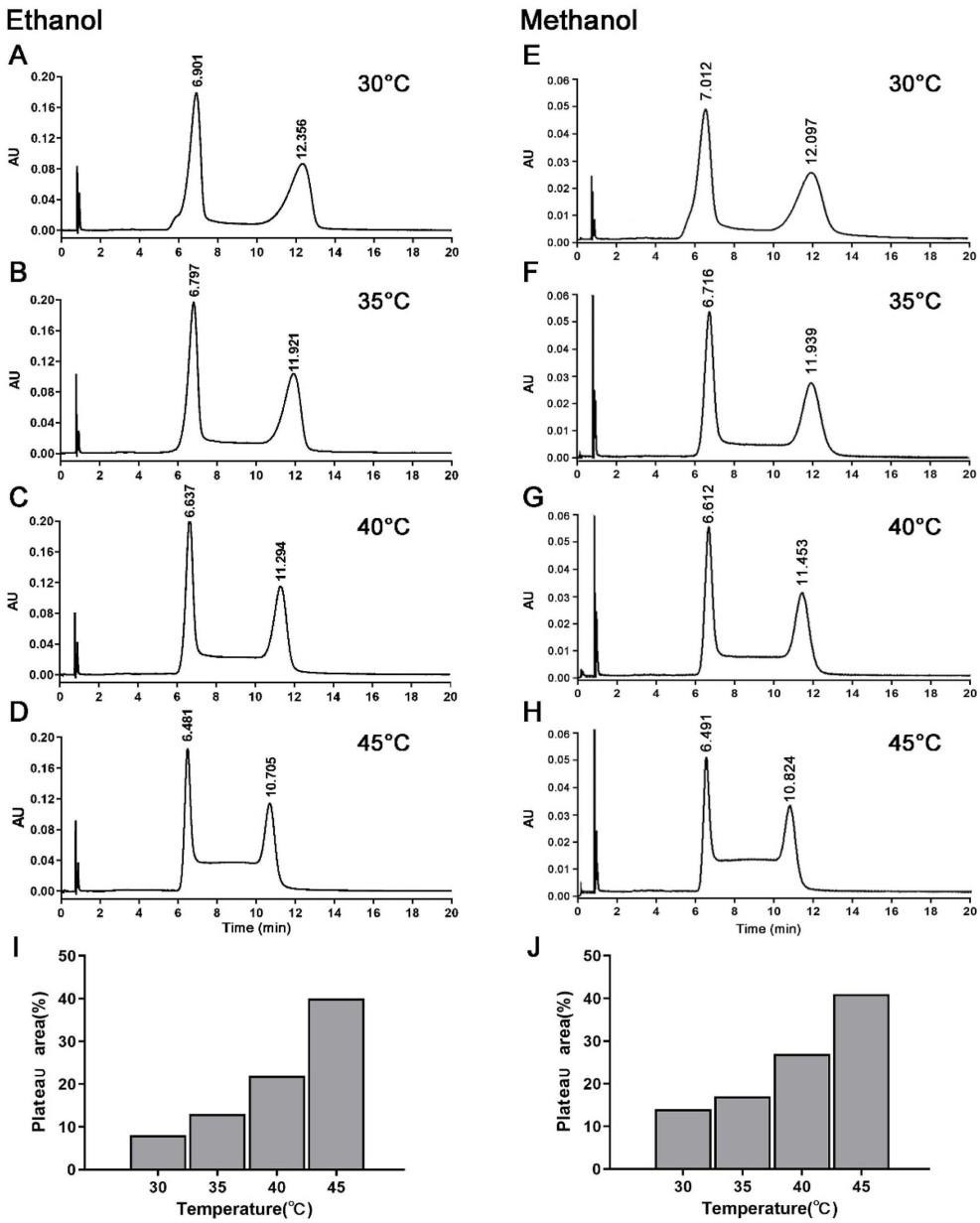

Fig. 5. Effect of column temperature on the separation of elagolix atropisomers. (A–D) ethanol, (E–H) methanol (30 %, v/v, in CO_2). (I, J) Corresponding area percentages of the interconversion plateau for ethanol and methanol, respectively..

3.2. Analytical method validation

The optimized SFC method was validated in terms of linearity, sensitivity, precision, accuracy, robustness, and solution stability.

The analytical validation results are summarized in *Table* 3. The total integrated response showed satisfactory linearity over the concentration range of 10~200 μg/mL, with a regression equation of $Y = 6071.4X + 32463$ and a coefficient of determination of 0.9998. The LOD and LOQ were 2.38 and 6.03 μg/mL, respectively. The total-response RSD was 1.43 % for repeatability and 1.06 % for the

Table 3. Summary of the analytical validation results for the developed SFC method

Parameter	Evaluation metric	Result	Acceptance criteria
Regression equation	Total integrated response versus nominal total elagolix concentration	$Y = 6071.4X + 32463$	—
Linear range	Five levels; three injections per level	10~200 μg/mL	—
Coefficient of determination	Linear regression and residual assessment	$r^2 = 0.9998$	$r^2 \geq 0.9990$
LOD	Based on S/N	2.38 μg/mL	S/N ≈ 3
LOQ	Based on S/N	6.03 μg/mL	S/N ≈ 10
Repeatability	Analyst A, Day1, six independent samples	Total-response RSD: 1.43 %; P_1/P_2 ratio RSD 1.73 %; R_S 1.8~2.1	RSD ≤ 2.0 %; $R_S \geq 1.5$
Intermediate precision	Analyst B, Day2, six independent samples	Total-response RSD: 1.06 %; P_1/P_2 ratio RSD 0.58 %; R_S 2.0~2.3	RSD ≤ 2.0 %; $R_S \geq 1.5$
	Combined results, n=12	Combined total-response RSD: 1.49 %; combined ratio RSD: 1.40 %; R_S: 1.8~2.3	RSD ≤ 2.0 %; $R_S \geq 1.5$
Accuracy, 80%	Total elagolix recovery; n=3	99.3 %; RSD 0.88 %	
Accuracy, 100%	Total elagolix recovery; n=3	100.4 %; RSD 1.76 %	95 %~105 %
Accuracy, 120%	Total elagolix recovery; n=3	100.6 %; RSD 1.29 %	
Robustness	Deliberate variation of three SFC parameters	Maximum P_1/P_2 ratio change: 1.24 %	Difference ≤ 2.0 %
Stability	48 h at 25 °C, n=6	Maximum P_1/P_2 ratio change: 1.61 %	Difference ≤ 2.0 %

second analyst/day, while the pooled RSD for all 12 independently prepared samples was 1.49 %. The corresponding Peak 1/Peak 2 area-ratio (P_1/P_2 ratio) RSDs were 1.73 %, 0.58 %, and 1.40 %, respectively, and the *R*s remained between 1.8 and 2.3. Mean recoveries at the 80 %, 100 %, and 120 % levels were 99.3 %, 100.4 %, and 100.6 %, with RSDs of 0.88 %, 1.76 %, and 1.29 %, respectively. Under deliberate variations in the chromatographic conditions, the maximum change in the Peak 1/Peak 2 area ratio was 1.24 %. After storage at 25 °C for 48 h, the maximum change in the Peak 1/Peak 2 area ratio was 1.61 %. The evaluated parameters met the predefined acceptance criteria, indicating that the method provides acceptable quantitative performance for total elagolix and consistent atropisomer separation.

3.3. Rotational energy barrier results and analysis

The relaxed potential energy surface scans in ethanol (*Fig.* 6F) reveal two distinct energy minima, each confirmed by frequency analysis to possess no imaginary frequencies (*Fig.* 6E). This confirms the existence of two stable conformers corresponding to the E and Z atropisomers (*Fig.* 6A, B)—which theoretically substantiates the appearance of two peaks in the SFC chromatogram. Between these two

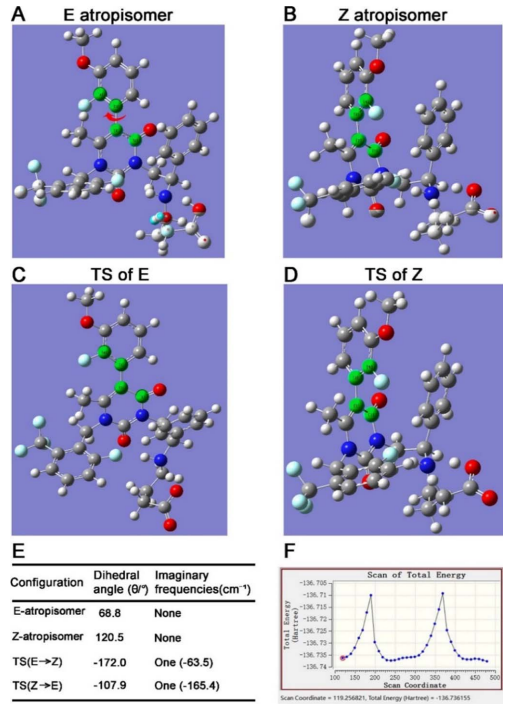

Configuration	Dihedral angle (θ/°)	Imaginary frequencies(cm⁻¹)
E-atropisomer	68.8	None
Z-atropisomer	120.5	None
TS(E→Z)	-172.0	One (-63.5)
TS(Z→E)	-107.9	One (-165.4)

Fig. 6. Optimized structures and potential energy surface of elagolix atropisomers in ethanol. (A) E-atropisomer and (B) Z-atropisomer. (C) Transition state for E→Z interconversion; (D) transition state for Z→E interconversion; (E) Dihedral angles and imaginary frequencies; (F) Potential energy surface scan. Red arrows indicate the rotational axis responsible for atropisomers, and the four carbon atoms defining the key dihedral angle shown in green.

Table 4. Kinetic and thermodynamic parameters for E/Z interconversion of elagolix atropisomers in ethanol and methanol at different temperatures

		E→Z			Z→E		
Solvent	T (K)	k_1 (S^{-1})	$t_{1/2}$ (h)	$\Delta G^{\ddagger}$ (kcal/mol)	k_1 (S^{-1})	$t_{1/2}$(h)	$\Delta G^{\ddagger}$ (kcal/mol)
Ethanol	303	1.98×10^{-6}	97.02	25.653	7.33×10^{-5}	2.63	23.480
	308	3.95×10^{-6}	48.74	25.665	1.34×10^{-4}	1.46	23.506
	313	7.68×10^{-6}	25.06	25.678	2.42×10^{-4}	0.80	23.532
Methanol	303	6.41×10^{-6}	30.04	24.947	4.85×10^{-5}	3.97	23.729
	308	1.22×10^{-5}	15.76	24.974	9.01×10^{-5}	2.14	23.751
	313	2.28×10^{-5}	8.44	25.001	1.65×10^{-4}	1.17	23.771

minima lies an energy maximum, verified by frequency analysis to exhibit a single imaginary frequency, corresponding to the transition state (TS) (*Fig.* 6C, D). The presence of this rotational energy barrier explains why separation is achievable under chromatographic conditions: interconversion between the two atropisomers requires overcoming the barrier, and the column temperature (or the overall chromatographic environment) provides the necessary energy for this transition. Consistent results were obtained in methanol, further supporting the theoretical model across different solvent systems.

Based on the optimized E/Z conformers and corresponding transition states, rotational energy barriers and kinetic parameters were calculated at different temperatures in ethanol and methanol. The calculated rotational energy barriers ranged from 23.48 to 25.68 kcal/mol (*Table* 4), placing elagolix into Class II of the LaPlante atropisomer classification (*Fig.* S2).[6,12] This classification indicates moderate configurational stability: the atropisomers are sufficiently stable to be resolved under appropriate chromatographic conditions, but interconversion may still occur under certain thermal or chromatographic environments. Therefore, the calculated barriers provide a kinetic basis for understanding why two distinct chromatographic peaks can be observed together with an interconversion plateau.

The calculated half-lives (0.8~97.0 h) indicated that elagolix atropisomers were not rapidly interconverting species. The half-lives were sufficiently long to allow chromatographic resolution, yet short enough to permit partial on-column interconversion, which was consistent with the observed interconversion plateau.

As temperature increased, the calculated rate constants k_1 increased and the corresponding half-lives decreased, this accelerated interconversion, which agreed with the experimentally observed enlargement of the interconversion plateau. Overall, the calculated rotational energy barriers and associated kinetic parameters provide a kinetic basis for understanding how chromatographic resolution can coexist with partial on-column interconversion of elagolix atropisomers.

4. Conclusion

This study established an efficient and environmentally friendly SFC method for resolving elagolix atropisomers. Using a Trefoil CEL2 column and a CO_2–ethanol mobile phase, the two atropisomer peaks were resolved within 15 min. Quantum chemical calculations showed rotational energy barriers of approximately 23~26 kcal/mol, placing elagolix in Class II of the LaPlante atropisomer classification. The temperature dependent changes in the interconversion plateau were consistent with the calculated kinetic trends. Overall, this experimental–computational strategy provides useful mechanistic insight into atropisomer separation and may support the development of analytical methods for other atropisomeric drugs.

Acknowledgments

This work was supported by the Shanghai postdoctoral

program at Shanghai Institute for Drug Control, and the Shanghai Municipal Commission of Science and Technology (Grant No. 20142202200).

Declaration of Interest

The authors declare that they have no known competing financial interests or personal relationships that could have appeared to influence the work reported in this paper.

References

1. Y. N. Lamb, *Drugs*, **78**(14), 1501-1508 (2018). https://doi.org/10.1007/s40265-018-0977-4
2. M. Ali, A. R. Sara, and A. Al Hendy, *Expert Rev. Clin. Pharmacol*., **14**(4), 427-437 (2021). https://doi.org/10.1080/17512433.2021.1900726
3. J. Muhammad, Y. Yusof, I. Ahmad, and M. N. Norhayati, *BMC Wom. Health*., **22**(1), 14-35 (2022). https://doi.org/10.1186/s12905-022-01596-2
4. S. Ciceri, D. Colombo, E. M. A. Fassi, P. Ferraboschi, G. Grazioso, P. Grisenti, M. Iannone, C. Castellano, and F. Meneghetti, *Molecules*., **28**(9), 3861-3882 (2023). https://doi.org/10.3390/molecules28093861
5. Z. Guo, Y. Chen, C. Q. Huang, T. D. Gross, J. Pontillo, M. W. Rowbottom, J. Saunders, S. Struthers, F. C. Tucci, Q. Xie, W. Wade, Y. F. Zhu, D. Wu, and C. Chen, *Bioorg. Med. Chem. Lett*., **15**(10), 2519-2522 (2005). https://doi.org/ 10.1016/j.bmcl.2005.03.057
6. S. R. LaPlante, P. J. Edwards, L. D. Fader, A. Jakalian, and O. Hucke, *Chem. Med. Chem*., **6**(3), 505-513 (2011). https://doi.org/ 10.1002/cmdc.201000485
7. L. Zhao, Z. Guo, Y. Chen, T. Hu, D. Wu, Y. F. Zhu, M. Rowbottom, T. D. Gross, F. C. Tucci, R. S. Struthers, Q. Xie, and C. Chen, *Bioorg. Med. Chem. Lett*., **18**(11), 3344-3349 (2008). https://doi.org/10.1016/j.bmcl.2008.04.029
8. S. T. Toenjes and J. L. Gustafson, *Future. Med. Chem*., **10**(4), 409-422 (2018). https://doi.org/ 10.4155/fmc-2017-0152
9. J. Clayden, W. J. Moran, P. J. Edwards, and S. R. LaPlante, *Angew. Chem. Int. Ed*., **48**(35), 6398-6401 (2009). https://doi.org/ 10.1002/anie.200901719
10. J. E. Smyth, N. M. Butler, and P. A. Keller, *Nat. Prod. Rep*., **32**(11), 1562-1583 (2015). https://doi.org/ 10.1039/c4np00121d
11. A. Lodola, S. Bertolini, M. Biagetti, S. Capacchi, F. Facchinetti, P. M. Gallo, A. Pappani, M. Mor, D. Pala, S. Rivara, F. Visentin, M. Corsi, and A. M. Capelli, *J. Med. Chem.*, **60**(10), 4304-4315 (2017). https://doi.org/10.1021/acs.jmedchem.7b00247
12. S. R. Laplante, L. D Fader, K. R. Fandrick, D. R. Fandrick, O. Hucke, R. Kemper, S. P. F. Miller, and P. J. Edwards, *J. Med. Chem*., **54**(20), 7005-7022 (2011). https://doi.org/10.1021/jm200584g
13. Y. Ogino, and T. Asahi, *J. Theor. Biol*., **373**(21), 117-131 (2015). https://doi.org/10.1016/j.jtbi.2015.03.011
14. State Food and Drug Administration (SFDA). Technical Guideline for Quality Control Research of Chiral Drugs, SFDA, Beijing, China (2006)
15. R. U. McVicker, and N. M. O'Boyle, *J. Med. Chem*., **67**(4), 2305-2320 (2024). https://doi.org/10.1021/acs.jmedchem.3c02239
16. M. Basilaia, M. H. Chen, J. Secka, and J. L. Gustafson, *Acc. Chem. Res*., **55**(20), 2904-2919 (2022). https://doi.org/ 10.1021/acs.accounts.2c00500
17. S. Patel, K. Sandha, A. Waingankar, and P. Jain, *Chem. Biol. Drug Des*., **101**(1), 138-157 (2023). https://doi.org/10.1111/cbdd.14155
18. S. Perreault, J. Chandrasekhar, and L. Patel, *Acc. Chem. Res*., **55**(18), 2581-2593 (2022). https://doi.org/10.1021/acs.accounts.2c00485
19. A. Zask, J. Murphy, and G. A. Ellestad, *Chirality*., **25**(5), 265-274 (2013). https://doi.org/10.1002/chir.22145
20. C. Nalbandian, D. Hecht, and J. Gustafson, *Synlett*., **27**(7), 977-983 (2016). https://doi.org/10.1055/s-0035-1561314
21. J. Wang, W. Zeng, S. Li, L. Shen, Z. Gu, Y. Zhang, J. Li, S. Chen, and X. Jia, *ACS Med. Chem. Lett*., **8**(3), 299-303 (2017). https://doi.org/10.1021/acsmedchemlett.6b00465
22. B. A. Lanman, A. T. Parsons, and S. G. Zech, *Acc. Chem. Res*., **55**(20), 2892-2903 (2022). https://doi.org/ 10.1021/acs.accounts.2c00479
23. C. J. Welch, *J. Chromatogra. A*., **666**(1), 3-26 (1994). https://doi.org/10.1016/0021-9673(94)80367-6
24. S. Bernardo-Bermejo, S. Adámez-Rodríguez, M. Castro-Puyana, and M. L. Marina, *Trend Anal. Chem*., **189**(2), 118256 (2025). https://doi.org/10.1016/j.trac.2025.118256

25. P. Borman, B. Boughtflower, K. Cattanach, and K. Crane, *Chirality*., **15**(1), S1-S12 (2003). https://doi.org/10.1002/chir.10260
26. S. Felletti, O. H. Ismail, C. D. Luca, V. Costa, F. Gasparrini, L. Pasti, N. Marchetti, A. Cavazzini, and M. Catani, *J. Chromatographia*., **82**(1), 65-75 (2019). https://doi.org/10.1007/s10337-018-3606-1
27. M. Ventura, *J. Pharm. Biomed*, **185**(10), 113227 (2020). https://doi.org/ 10.1016/j.jpba.2020.113227
28. K. S. Watts, P. Dalal, A. J. Tebben, D. L. Cheney, and J. C. Shelley, *J. Chem. Inf. Model*., **54**(10), 2680-2696 (2014). https://doi.org/10.1021/ci5001696
29. M. J. Frisch, G. W. Trucks, and H. B. Schlegel, Gaussian 16, *Revision C.01, Gaussian*, Inc., Wallingford, CT, USA (2019)
30. C. Bannwarth, S. Ehlert, and S. Grimme, *J. Chem. Theory. Comput*., **15**(3), 1652-1671 (2019). https://doi.org/10.1021/acs.jctc.8b01176
31. I. T. Lima, R. F. C. Gomes, E. N. C. Paura, P. F. Provasi, R. Gester, and A. Rodrigues da Cunha, *J. Mol. Model*., **30**(9), 314-329(2024). https://doi.org/10.1007/s00894-024-06108-7
32. T. Lu and Q. Chen, *Comput. Theor. Chem*., **1200**(1), 113249 (2021). https://doi.org/10.1016/j.comptc.2021.113249
33. A. D. Becke, *Phys. Rev. A Gen. Phys*., **38**(6), 3098-3100 (1988). https://doi.org/10.1103/physreva.38.3098
34. A. D. Becke, *J. Chem. Phys*., **98**(7), 5648-5652 (1993). https://doi.org/10.1063/1.464913
35. O. Trapp, *Anal. Chem*., **78**(1), 189-198 (2006). https://doi.org/ 10.1021/ac051655r
36. O. Trapp, *Chirality*., **18**(7), 489-497 (2006). https://doi.org/10.1002/chir.20276
37. O. Trapp, *J. Chromatogr B. Analyt. Technol. Biomed. Life*., **875**(1), 42-47 (2008). https://doi.org/10.1016/j.jchromb.2008.07.047
38. O. Trapp, S. Bremer, and S. K. Weber, *Anal. & Bioanal. Chem*., **395**(6), 1673-1679 (2009). https://doi.org/10.1007/s00216-009-2993-4
39. I. D'Acquarica, F. Gasparrini, M. Pierini, C. Villani, and G. Zappia, *J. Sep. Sci*., **29**(10), 1508-1516 (2006). https://doi.org/10.1002/jssc.200600129
40. O. Trapp, G. Schoetz, and V. Schurig, *Chirality*., **13**(8), 403-414 (2001). https://doi.org/10.1002/chir.1052
41. C. Wolf, *Chem. Soc. Rev*., **34**(7), 595-608 (2005). https://doi.org/10.1039/b502508g
42. W. A. König, B. Gehrcke, T. Runge, and C. Wolf, *J. High Resol. Chromatogr*., **16**(6), 376-378 (1993). https://doi.org/10.1002/jhrc.1240160609